



Effect of alkali treatments on apatite formation of microarc-oxidized coating on titanium alloy surface

Guo-liang ZHAO, Long XIA, Bo ZHONG, Song-song WU, Liang SONG, Guang-wu WEN

School of Materials Science and Engineering, Harbin Institute of Technology at Weihai, Weihai 264209, China

Received 10 April 2014; accepted 29 July 2014

Abstract: Alkali treatments with three concentrations were used to modify a microarc-oxidized (MAO) coating on titanium alloy surface in order to further improve its surface bioactivity. Morphology, chemical compositions and phase constituents, roughness, contact angle and apatite induction of the alkali-treated coatings were studied and compared. Scanning electron microscope (SEM) was applied to observe the morphologies, X-ray diffraction (XRD) and X-ray photoelectron spectroscopy (XPS) were used to detect the phase constituents and chemical compositions, a surface topography profilometer was used to analyze the surface roughness, and contact angle was measured by liquid drop method. Alkali treatments result in the formation of $\text{Na}_2\text{Ti}_6\text{O}_{13}$ and $\text{Na}_2\text{Ti}_3\text{O}_7$ phase on the MAO coating, which leads to the increase of surface roughness and the decrease of contact angle. Experimental results showed that the apatite induction of the alkali-treated coatings was dependent on the applied alkali concentrations during treatments, and Na^+ concentration can promote the formation of apatite phase.

Key words: titanium alloy; micro-arc oxidation; alkali treatment; alkali concentration; Ti—OH group; apatite; formation

1 Introduction

Titanium and its alloys are promising biomedical metal materials owing to their good biocompatibility, corrosion resistance and mechanical properties such as strength, hardness and wear resistance, which are widely used in dental and orthopedic implant applications [1–3]. In recent years, the development of a series of new titanium alloys with elastic moduli matching natural bone has brought more bright future to further biomedical applications [4–6].

However, the inert surfaces of titanium and its alloys could be a major obstacle to the formation of efficient bond with living bone and new tissue on their surfaces at the early stage of implantation and even result in the failure of implantation [7,8]. In order to enhance the bioactivity of titanium implants, many attempts have been made to modify the composition and chemistry of the titanium surfaces, such as plasma-spraying, laser cladding, electrophoretic deposition, plasma assisted chemical vapour deposition technique, and biomimetic technique [9–13]. Micro-arc oxidation (MAO) is another simple, controllable and effective method to form

bioceramic coatings on light metals such as titanium and its alloys [14–16]. The process combines electrochemical oxidation with a high voltage spark treatment in an aqueous electrolytic bath, which also contains modifying elements in the form of dissolved salts (e.g., calcium and phosphorous). Previous studies showed that Ca and P elements can further crystallize into calcium phosphate or even directly formed hydroxyapatite (HA) [17,18]. Another advantage of this process is that the MAO coatings have porous nature which can enhance the anchorage of implants to the bone [19]. In addition, MAO can form coatings on metrically complex surface, which is of importance for enabling the bone-bonding ability of implants [20].

Generally, it is difficult for MAO technique alone to provide sufficient bioactivity within a relative short time [21,22]. The alkali treatment has attracted increasing interest due to its simplicity and efficiency. Amorphous sodium titanate hydrogel can form on the titanium and its alloy surfaces after alkali treatments and the treated surfaces can induce apatite formation after soaking for a certain time in a simulated body fluid (SBF) [23,24]. It was reported that the formation of Ti—OH groups on alkali treated titanium surfaces was the major factor of

Foundation item: Projects (51172050, 51102060, 51302050) supported by the National Natural Science Foundation of China; Project (HIT.ICRST.2010009) supported by the Fundamental Research Funds for Central Universities, China, Project (HIT.NSRIF.2014129) supported by the Natural Scientific Research Innovation Foundation in Harbin Institute of Technology, China

Corresponding author: Long XIA; Tel: +86-631-5687577; E-mail: xialonghit@gmail.com

DOI: 10.1016/S1003-6326(15)63710-4

induction of apatite [25,26]. The combination of MAO process with alkali treatment may be a more desirable solution to produce high bioactive materials surfaces [22]. Moreover, it has a promising application prospect in industrial production due to the simplicity and low cost.

Our prior study [27] suggested that the alkali treatment accelerated the formation of apatite on the micro-arc oxidized titanium alloy surface. However, the effect of alkali concentrations on the apatite formation has not been studied. In this work, the surface morphology, chemical and phase compositions and wetting ability of the MAO coatings treated by alkali solutions with various concentrations were examined. Apatite-formation abilities of different alkali-treated MAO surfaces were compared and the probable influencing factors were discussed.

2 Experimental

2.1 Preparation of MAO coating

The preparation of the MAO coating has reported in Ref. [27]. T2448 alloy plates (50 mm × 30 mm × 5 mm) were used as substrates for the MAO process. The mole fractions of alloying elements Nb, Zr and Sn were 24.1%, 3.92% and 7.85%, respectively [5]. During the MAO process, the T2448 plates were employed as anodes, while stainless steel plates were used as cathodes. An electrolyte was prepared by dissolving $\text{Ca}(\text{CH}_3\text{COO})_2 \cdot \text{H}_2\text{O}$ (6.3 g/L), $\text{Ca}(\text{H}_2\text{PO}_4)_2 \cdot \text{H}_2\text{O}$ (13.2 g/L) and NaOH (18 g/L) into deionized water. The applied voltage, frequency, duty cycle and oxidizing time were 450 V, 600 Hz, 8.0% and 5 min, respectively. The system temperature was maintained below 40 °C by a water bath. The samples just after the MAO treatment hereafter are abbreviated as the MAO.

2.2 Alkali treatment

The MAO samples were treated in 20 mL of 5, 10 and 15 mol/L NaOH solutions at room temperature for 48 h, respectively. Then, the specimens were gently washed with deionized water and dried at room temperature. The MAO samples after alkali treatments with concentrations of 5, 10 and 15 mol/L were labeled as the MAO-5M, MAO-10M and MAO-15M, respectively.

2.3 Immersion in SBF

Both of the MAO and the alkali treated specimens were soaked in 20 mL of simulated body fluid (SBF) for 7, 14, 21 and 28 d. SBF solution was refreshed every other day. The SBF was prepared by dissolving reagent-grade chemicals of NaCl, NaHCO_3 , KCl, $\text{K}_2\text{HPO}_4 \cdot 3\text{H}_2\text{O}$, $\text{MgCl}_2 \cdot 6\text{H}_2\text{O}$, CaCl_2 and Na_2SO_4 into distilled water in order and buffering at pH 7.40 with tris (hydroxymethyl)

aminomethane and dilute HCl at 37 °C. The ionic concentrations of Na^+ , K^+ , Mg^{2+} , Ca^{2+} , Cl^- , HCO_3^{2-} , HPO_4^{2-} and SO_4^{2-} of SBF were 142.0, 5.0, 1.5, 2.5, 147.8, 4.2, 1.0 and 0.5 mmol/L, respectively.

2.4 Characterization

The surface morphologies of all the samples were observed by scanning electron microscopy (SEM; Tescan Vega II, the Czech Republic). The surface roughness (R_a) of the MAO coating and alkali-treated coatings was analyzed with a surface topography profilometer (Talysurf 5P-120, Rank Taylor Hobson, England). Wetting angle was measured by liquid drop method (using distilled water) on a contact angle goniometer (DSA100, Kruss, Germany). Five measurements were made on each sample.

Chemical compositions and ion concentrations of the MAO sample surfaces before and after alkali treatment were identified by X-ray photoelectron spectroscopy (XPS; Thermal ESCALAB 250, VG, England). Crystalline phases of the surfaces of the alkali-treated coatings were detected by a X-ray diffraction (XRD; D8 ADVANCE, Bruker, Germany) using a Cu K_α radiation in the regular range $2\theta=10^\circ\text{--}90^\circ$ with an accelerating voltage of 40 kV, a current of 100 mA and a scanning speed of 4 (°)/min. The chemical compositions of the sample surface after immersion in SBF were detected by an energy dispersive X-ray spectrometer (EDS; EDAX-Genesis, USA) equipped on SEM system.

3 Results and discussion

3.1 Morphologies of alkali-treated MAO coatings

In order to investigate the influence of alkali concentration on the MAO coating, three alkali concentrations of 5, 10 and 15 mol/L were applied during the modifications. Figure 1 shows the surface morphologies of the MAO coating before and after alkali treatments. It is clear that after alkali treatments, the surface morphologies of the coatings are changed remarkably although the surfaces are still porous. After alkali treatments, the relatively smooth surface of the coating becomes rough obviously. In addition, the surface morphologies are different significantly after alkali treatments with different concentrations. Squama-like granules with the size of about 100 nm can be seen on the surface of MAO-5M coating (Figs. 1(c) and (d)). A small amount of thin cracks are present around the pores. With increasing the alkali concentration to 10 mol/L, a network structure of nanoflakes with the thickness of less than 100 nm distributes homogeneously on MAO-10M coating surface (Figs. 1(e) and (f)). The pores achieved during microarc oxidation become

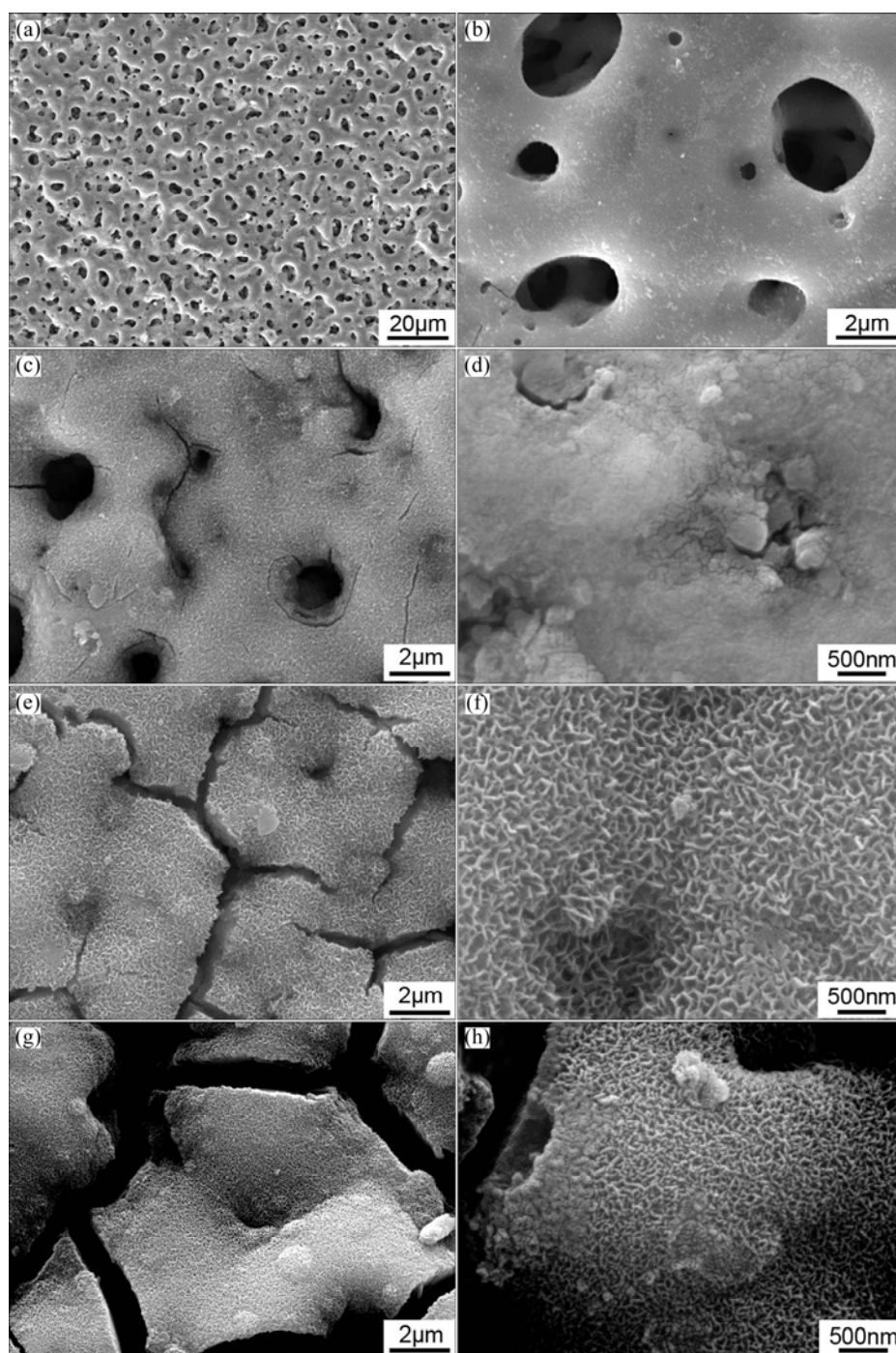


Fig. 1 Surface morphologies of MAO coating before and after alkali treatments: (a,b) MAO; (c,d) MAO-5M; (e,f) MAO-10M; (g,h) MAO-15M

blurred because they are mostly filled by some kind of deposits. The cracks become larger and deeper than those on the surface of MAO-5M. The deposition morphology of MAO-15M coating is very similar with that of MAO-10M, but the case of cracks is more serious (Figs. 1(g) and (h)). It must be pointed out that large and deep shrinkage cracks appearing in the modified layer of the alkali-treated MAO coatings with higher alkali concentrations could lead to delamination of the coating

surface during clinical applications [28]. Therefore, the applied alkali concentration must be controlled under a certain scale.

The changes appearing on the MAO surface are the result of etching of the NaOH aqueous solutions. After treatment, hydrated sodium titanate gel layer can form on the surface of titanium oxide layer, which always shows network structure [22,29]. The cracks are resulted from shrinkage of the sodium titanate layer due to dehydration

during drying. With the increase of the concentration of alkali, the amount of corrosion products increases and the deposition layer becomes thicker and thicker. Therefore, the cracks formed during drying process are larger and deeper.

3.2 Chemical and phase compositions of alkali-treated MAO coatings

Figure 2 shows the XRD patterns of the alkali-treated MAO coatings. XRD patterns reveal that the crystalline phase compositions of the three alkali-treated coatings are almost the same. Low peaks suggest that the modified layers of the MAO coatings are mostly composed of amorphous phases. The presence of $\text{Na}_2\text{Ti}_6\text{O}_{13}$ and $\text{Na}_2\text{Ti}_3\text{O}_7$ implies the reaction between titanium oxides in MAO coating with NaOH during alkali treatment process. Thereby, it can be inferred that the nanostructure observed in Fig. 1 should come from the deposition of sodium titanate. Moreover, the intensity of sodium titanate peaks increases with the increase of the alkali concentration, indicating the increase of the amount of sodium titanate phase.

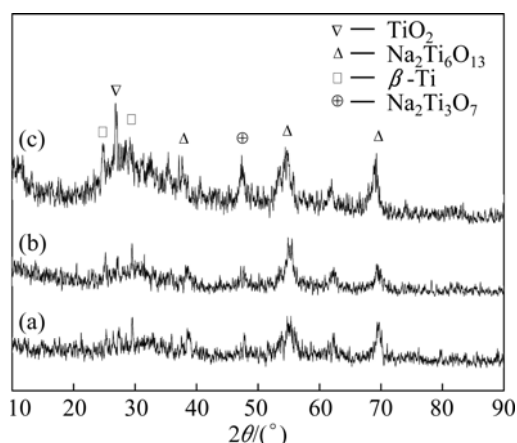


Fig. 2 XRD patterns of alkali-treated MAO coatings: (a) MAO-5M; (b) MAO-10M; (c) MAO-15M

The chemical compositions of modified layers detected by XPS are listed in Table 1. They mainly include O, Ti, Na, Ca and Nb. It is worth noting that the Na concentrations in all the modified coatings are higher than that in the original MAO coating (Na: 2.1%), and Ca and P concentrations in them are lower than that in the MAO coating (Ca: 8.8%, P: 5.5%). With increasing alkali concentration, Na concentration in the modified coatings increases. In contrast, Ca and P concentrations decrease. The increase of Na concentration should be attributed to the formation and growth of sodium titanium layer. As we know, when titanium oxide is exposed to NaOH aqueous solution, it reacts with NaOH and forms HTiO_3^- . The negatively charged hydrate titanate reacts with Na^+ ions to form sodium titanate in

order to maintain electrical neutrality [22,27]. The dissolution of Ca and P into NaOH aqueous solution resulted in the decrease of them [29,30].

Table 1 Elemental compositions detected by XPS on surfaces of alkali-treated coatings

Coating	Mole fraction/%						
	Ti	Nb	Sn	Na	Ca	P	O
MAO-5M	19.24	1.60	0.12	4.58	6.84	0.14	67.48
MAO-10M	16.58	1.64	0.29	7.23	6.02	0.12	68.12
MAO-15M	19.65	1.56	0.15	8.25	3.45	0.09	66.85

3.3 Roughness and wetting ability of alkali-treated MAO coatings

It has already been mentioned above that the surface morphologies of the MAO coating changed significantly after alkali treatments. The alkali-treated coating surfaces were rougher than that before treatments (as shown in Fig. 1). Figure 3 exhibits bar charts of roughness and contact angle of alkali-treated MAO coatings. For comparison, the bar charts of roughness and contact angle of the titanium alloy and the MAO coating are also provided. After alkali treatments, the roughness values of the coatings increase. The increase of roughness of the coating surface treated with higher concentration is

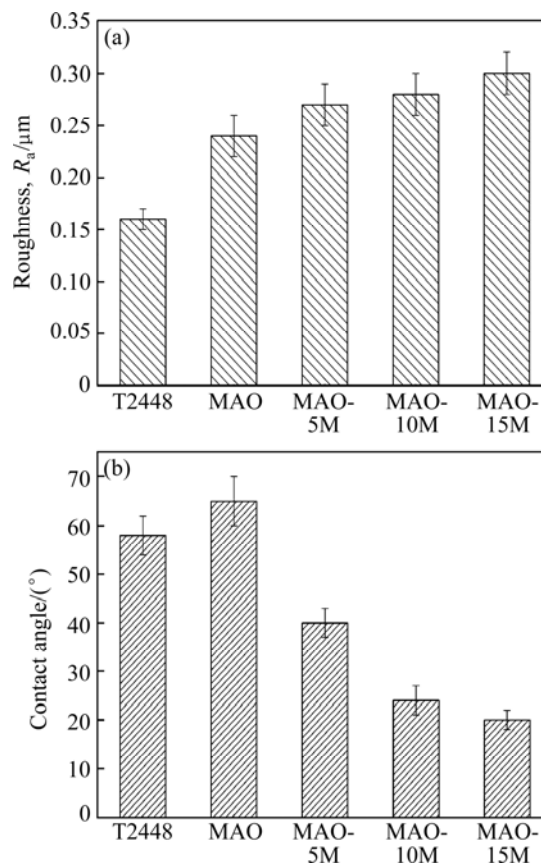


Fig. 3 Roughness and contact angle of alkali-treated MAO coatings: (a) Roughness; (b) Contact angle

more remarkable than that treated with lower concentrations ($p < 0.05$) (Fig. 3(a)). It can be inferred from the surface morphologies that the formation of network of nanoflakes and appearance of cracks on the surface should be responsible for the increase of the roughness.

Contrary to the change tendency of roughness, the contact angles of the alkali-treated coatings decrease more remarkably than those of the MAO coating ($p < 0.01$). Increasing alkali concentration can further decrease the contact angles ($p < 0.05$) (Fig. 3(b)). It is well known that the decrease of contact angles indicates the increase of wetting ability. Therefore, the alkali treatments remarkably increase the wetting ability of the MAO coating ($p < 0.01$). In contrast to the treatment with lower alkali concentration (5 mol/L), the treatment with higher alkali concentration (10 mol/L) achieves better wetting results ($p < 0.01$). Further increasing alkali concentration, the wetting ability of the coating increases slightly ($p < 0.05$).

3.4 Apatite induction ability of alkali-treated MAO coatings

In vivo bioactivity of coatings can be evaluated through soaking the sample in SBF and examining the formation of apatite. Figure 4 shows the morphologies of the alkali-treated MAO coatings after immersion in SBF

for 7, 14 and 28 d, respectively. After immersion in SBF for 7 d, no obvious change appears on the surface of MAO-5M coating (Fig. 4(a)). A few of spherical depositions appear on the surface of MAO-5M coating soaked in SBF for 14 d (Fig. 4(b)). After immersion for 28 d, more depositions form on its surface (Fig. 4(c)). Figures 4(d)–(f) show the morphologies of MAO-10M coating after immersion in SBF for 7, 14 and 28 d, respectively. After immersion for 7 d, a large amount of spherical depositions with diameter of about 500 nm are observed. After immersion for 14 d, the size and amount of spherical depositions increase. The deposits with porous morphology mostly cover the surface of MAO-10M coating. Further immersion to 28 d, the spherical deposits continue to grow larger, joining and integrating with each other, which cover the surface of the coating completely.

Figures 4(g)–(i) show the morphologies of MAO-15M coating after immersion in SBF for 7, 14 and 28 d, respectively. The amount of deposits on the surface of MAO-15M coating soaked for 7 d is obviously more than that on the surface of MAO-10M after the same time immersion. After immersion for 14 d, an acanthosphere-like deposition layer forms on the surface of the coating. Further immersion to 28 d, the deposit continues to grow larger and the deposit layer becomes thicker.

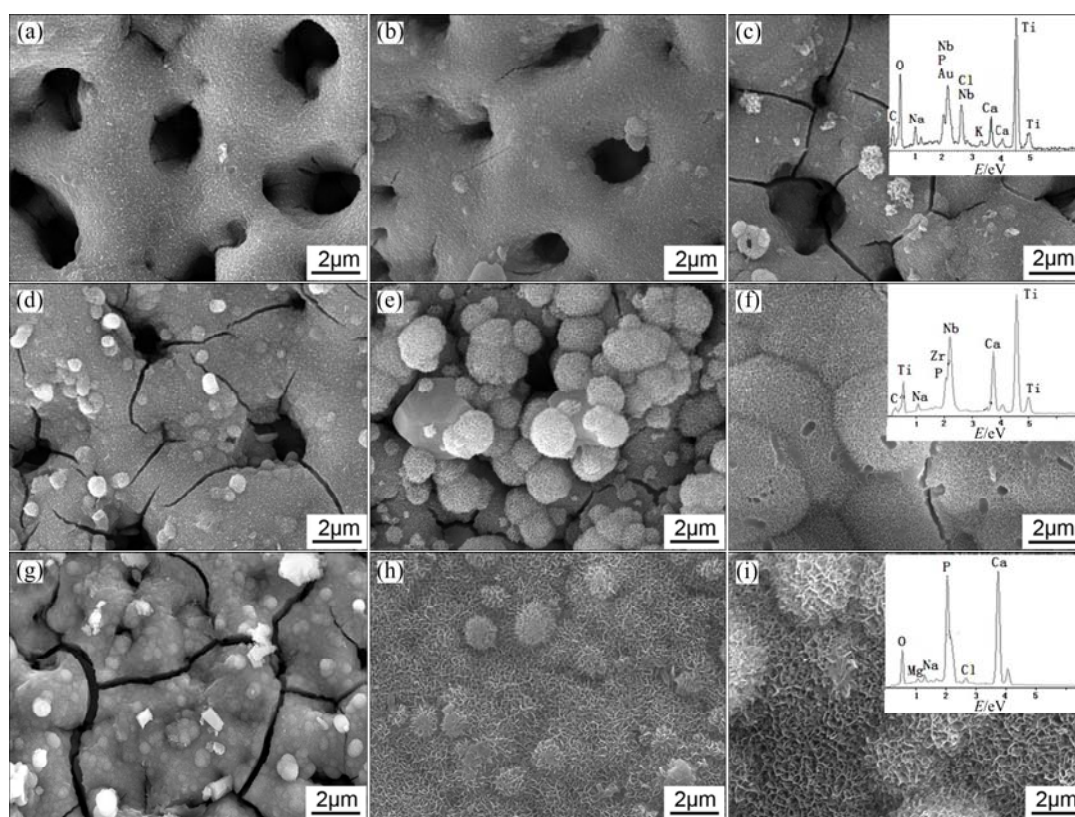


Fig. 4 Morphologies of alkali-treated MAO coatings after immersion in SBF for 7 d (a, d, g), 14 d (b, e, h) and 28 d (c, f, i), respectively: (a–c) MAO-5M; (d–f) MAO-10M; (g–i) MAO-15M

EDS results of the three coatings soaked in SBF for 28 d indicate that all the deposits consist of Ca, P and O. Ti and Nb elements can be detected from the surfaces of MAO-5M and MAO-10M after immersion for 28 d, but these elements do not appear in the MAO-15M sample. This result indicates that the deposition layer on MAO-15M is remarkably thicker than that on the other alkali-treated coatings after immersion for 28 d.

The deposits formed on the MAO-10M coating are apatite, which has been certified in prior study [29]. Accordingly, it can be deduced that the depositions formed on the other alkali-treated coating after immersion in SBF are also apatite because of the similar chemical composition on the surface of all of the coatings. Apatite formation mechanism has been also explained in other literatures [26,29–31]. After alkali treatments, sodium titanate layer forms on the MAO coating. When the alkali-treated coatings soak in SBF, Ti—OH groups form on the surface of the coatings via ion exchange between Na^+ in the coatings and H_3O^+ in SBF solution. The electrostatic potential energy resulting from OH^- groups make positively charged Ca^{2+} adhere to the coating surface. Ca^{2+} absorbs PO_4^{3-} and CO_3^{2-} in SBF solution. With increasing immersion time, the supersaturation of Ca^{2+} , PO_4^{3-} and CO_3^{2-} forms around Ti—OH groups, which triggers nucleation of apatite. Once apatite nuclei forms, Ca^{2+} , PO_4^{3-} and CO_3^{2-} near the nuclei grow on the basis of the nuclei via self-assembly.

According to the mentioned above, the MAO coatings treated with higher concentration have higher apatite induction abilities. This mechanism could be discussed as follows. Firstly, the coatings treated with higher Na^+ concentration can provide higher wetting ability (Fig. 3). When soaked in SBF solution, the ions could easily contact the surface of these coatings, which benefits the realization of electrostatic adherence between ions in the coating surfaces and that in SBF. Secondly, higher Na^+ concentrations are present on the surfaces of these coatings. The release of Na^+ from coatings to SBF solution is the key of the formation of Ti—OH groups. The formation of Ti—OH groups is the basis of apatite nucleation. Therefore, more Na^+ ions mean that more Ti—OH groups might form on the surface of these coatings, which could trigger to form more apatite nuclei. Thirdly, the microstructures on the surface of these coatings could provide better nucleation spaces. It is well known that nano-sized nucleation is usually required for inorganic formation in natural biomineralized systems. As shown in Fig. 1, the surfaces of MAO-10M and MAO-15M coatings are covered by a large amount of nanoflakes. The nanostructures made up of the nanoflakes could become the perfect nucleation spaces for apatite.

4 Conclusions

1) Alkali treatments are successfully applied on the MAO coating of T2448 titanium alloy. Sodium titanate phases form on the alkali-treated MAO coatings, demonstrating nanoflake characteristics with the thickness of less than 100 nm.

2) The alkali concentrations have important influence on the original MAO coating. The coating surfaces have more perfect microstructure, better wetting ability with increasing the alkali concentration during treatments.

3) Sodium titanate layer formed on the MAO coating after alkali treatments provide more nucleation sites for apatite when immersed in SBF. The coatings treated by high alkali concentrations process excellent apatite induction properties. However, when the concentration of alkali is as high as 15 mol/L, the excessive alkali could result in the appearance of more and larger cracks which would damage the stability of the coatings in applications.

Acknowledgements

The authors would like to thank Dr. Ya-ming WANG of Harbin Institute of Technology for his friendly help of this work. We also would like to acknowledge financial support provided by program of excellent Team in Harbin Institute of Technology and the financial support from Yunshan Carbon Industry Co., Ltd.

References

- [1] KRISHNA B V, BOSE S, BANDYOPADHYAY A. Low stiffness porous Ti structures for load-bearing implants [J]. *Acta Biomaterialia*, 2007, 3: 997–1006.
- [2] MORAIS L S, SERRA G G, MULLER C A, ANDRADE L R, PALERMO E F A, ELIAS C N, MEYERS M. Titanium alloy mini-implants for orthodontic anchorage: Immediate loading and metal ion release [J]. *Acta Biomaterialia*, 2007, 3: 331–339.
- [3] GEETHA M, SINGH A K, ASOKAMANI R, DOGIA A K. Ti based biomaterials, the ultimate choice for orthopaedic implants—A review [J]. *Progress in Materials Science*, 2009, 54: 397–425.
- [4] LI S J, CUI T C, HAO Y L, YANG R. Fatigue properties of a metastable β -type titanium alloy with reversible phase transformation [J]. *Acta Biomaterialia*, 2008, 4: 305–317.
- [5] DAI Shui-juan, WANG Yu, CHEN Feng, YU Xin-quan, ZHANG You-fa. Influence of Zr content on microstructure and mechanical properties of implant Ti–35Nb–4Sn–6Mo–xZr alloys [J]. *Transactions of Nonferrous Metals Society of China*, 2013, 23(5): 1299–1303.
- [6] LIU F, WANG F, SHIMIZU T, IGARASHI K, ZHAO L. Hydroxyapatite formation on oxide films containing Ca and P by hydrothermal treatment [J]. *Ceramics International*, 2006, 32: 527–531.
- [7] TAKAO H. Biofunctionalization of titanium for dental implant [J]. *Japanese Dental Science Review*, 2010, 46: 93–98.
- [8] LIU F, WANG F, SHIMIZHU T, IGARASHI K, ZHAO L. Formation of hydroxyapatite on Ti–6Al–4V alloy by microarc oxidation and hydrothermal treatment [J]. *Surface and Coatings Technology*, 2005,

- 199: 220–224.
- [9] ZHAO G, XIA L, WEN G, SONG L, WANG X, WU K. Microstructure and properties of plasma-sprayed bio-coatings on a low-modulus titanium alloy from milled HA/Ti powders [J]. Surface and Coatings Technology, 2012, 206: 4711–4719.
- [10] YANG S, LI W H, MAN H C. Laser cladding of HA/Ti composite coating on NiTi alloy [J]. Surface Engineering, 2013, 29: 409–431.
- [11] WANG J, HUANG C, WAN Q, CHEN Y, CHAO Y. Characterization of fluoridated hydroxyapatite/zirconia nano-composite coating deposited by a modified electrocodeposition technique [J]. Surface and Coatings Technology, 2010, 204: 2576–2582.
- [12] CHENG X M, NIE B M, KUMAR S. Preparation and bioactivity of SiO₂(2) functional films on titanium by PACVD [J]. Transactions of Nonferrous Metals Society of China, 2008, 18(3): 627–630.
- [13] ZHANG E, ZOU C, ZENG S. Preparation and characterization of silicon-substituted hydroxyapatite coating by a biomimetic process on titanium substrate [J]. Surface and Coating Technology, 2009, 203: 1075–1080.
- [14] LUO Qiang, CAI Qi-zhou, LI Xin-wei, PAN Zhen-hua, LI Yu-jie, CHEN Xi-di, YAN Qing-song. Preparation and characterization of ZrO₂/TiO₂ composite photocatalytic film by micro-arc oxidation [J]. Transactions of Nonferrous Metals Society of China, 2013, 23(10): 2945–2950.
- [15] LI Hong-xia, SONG Ren-guo, JI Zhen-guo. Effects of nano-additive TiO₂ on performance of micro-arc oxidation coatings formed on 6063 aluminum alloy [J]. Transactions of Nonferrous Metals Society of China, 2013, 23(2): 406–411.
- [16] GUO Hui-xia, MA Ying, WANG Jing-song, WANG Yu-shun, DONG Hai-rong, HAO Yuan. Corrosion behavior of micro-arc oxidation coating on AZ91D magnesium alloy in NaCl solutions with different concentrations [J]. Transactions of Nonferrous Metals Society of China, 2012, 22(7): 1786–1793.
- [17] WEI D Q, ZHOU Y, JIA D C, WANG Y M. Effect of heat treatment on the structure and in vitro bioactivity of microarc-oxidized (MAO) titania coatings containing Ca and P ions [J]. Surface and Coatings Technology, 2006, 201: 8723–8729.
- [18] LI L H, KIM H W, LEE S H, KONG Y M, KIM H E. Biocompatibility of titanium implants modified by microarc oxidation and hydroxyapatite coating [J]. Journal of Biomedical Materials Research A, 2005, 73: 48–54.
- [19] PAITAL S R, DAHOTRE N B. Calcium phosphate coatings for bio-implant applications: Materials, performance factors, and methodologies [J]. Materials Science and Engineering R: Reports, 2009, 66: 1–70.
- [20] YAO Z Q, IVANISENKO Y, DIEMANT T, CARON A, CHUVILIN A, JIANG J Z, VALIEV R Z, QI M, FECHT H J. Synthesis and properties of hydroxyapatite-containing porous titania coating on ultrafine-grained titanium by micro-arc oxidation [J]. Acta Biomaterialia, 2010, 6: 2816–2825.
- [21] ISHIZAWA H, OGINO M. Formation and characterization of anodic titanium oxide films containing Ca and P [J]. Journal of Biomedical Materials Research, 1995, 29: 65–72.
- [22] WEI D Q, ZHOU Y, WANG Y B, MENG Q C, JIA D C. Structure and apatite formation of microarc oxidized TiO₂-based films before and after alkali-treatment by various alkali concentrations [J]. Surface and Coatings Technology, 2008, 202: 5012–5019.
- [23] KIM H M, MIYAJI F, KOKUBO T, NAKAMURA T. Preparation of bioactive Ti and its alloys via simple chemical surface treatment [J]. Journal of Biomedical Materials Research, 1996, 32: 409–417.
- [24] KIM H M, MIYAJI F, KOKUBO T, NAKAMURA T. Effect of heat treatment on apatite-forming ability of Ti metal induced by alkali treatment [J]. Journal of Materials Science: Materials in Medicine, 1997, 8: 341–347.
- [25] CHEN Y K, ZHENG X B, JI H, DING C X. Effect of Ti-OH formation on bioactivity of vacuum plasma sprayed titanium coating after chemical treatment [J]. Surface and Coatings Technology, 2007, 202: 494–498.
- [26] ZHANG P, ZHANG Z G, LI W, ZHU M. Effect of Ti-OH groups on microstructure and bioactivity of TiO₂ coating prepared by micro-arc oxidation [J]. Applied Surface Science, 2013, 268: 381–386.
- [27] WEI D Q, ZHOU Y, JIA D C, WANG Y M. Characteristic and in vitro bioactivity of a microarc-oxidized TiO₂-based coating after chemical treatment [J]. Acta Biomaterialia, 2007, 3: 817–827.
- [28] LIN J G, LI Y C, WONG C S, HODGSON P D, WEN C E. Degradation of the strength of porous titanium after alkali and heat treatment [J]. Journal of Alloys and Compounds, 2009, 485: 316–319.
- [29] YAN Y, HAN H, LU C G. The effect of chemical treatment on apatite-forming ability of the macroporous zirconia films formed by micro-arc oxidation [J]. Applied Surface Science, 2008, 254: 4833–4839.
- [30] PAN Y K, CHEN C Z, WANG D G, LIN Z G. Preparation and bioactivity of micro-arc oxidized calcium phosphate coatings [J]. Materials Chemistry and Physics, 2013, 141: 842–849.
- [31] ZHU W J, FANG Y J, ZHENG H D, TAN G X, CHENG H M, NING C Y. Effect of applied voltage on phase components of composite coatings prepared by micro-arc oxidation [J]. Thin Solid Films, 2013, 544: 79–82.

碱处理对钛合金表面微弧氧化涂层中磷灰石形成的影响

赵国亮, 夏龙, 钟博, 吴松松, 宋亮, 温广武

哈尔滨工业大学(威海) 材料学院, 威海 264209

摘要: 使用 3 种不同浓度的氢氧化钠溶液对钛合金表面的微弧氧化涂层(MAO)进行改性处理, 以提高微弧氧化涂层的生物活性。通过分析经不同浓度碱溶液处理后样品的微观形貌、化学成分、相组成、表面粗糙度、接触角和磷灰石的形成程度等因素, 研究碱处理对微弧氧化涂层的影响。实验结果表明, 碱处理后的微弧氧化涂层中生成了 Na₂Ti₆O₁₃ 和 Na₂Ti₃O₇ 相, 这两相的生成增加了微弧氧化涂层的表面粗糙度, 减小了模拟体液与涂层的接触角。因此, 采用不同浓度碱处理能够促进微弧氧化涂层中磷灰石的形成, 使涂层表面的生物活性增加。

关键词: 钛合金; 微弧氧化; 碱处理; 碱浓度; Ti—OH 基团; 磷灰石; 形成

(Edited by Yun-bin HE)